Assessment of ballast layer under multiple field conditions in China

Guo, Yunlong; Wang, Shilei ; Jing, Guoqing; Yang, Fei; Liu, Guixian ; Qiang, Weile; Wang, Yan

Assessment of ballast layer under multiple field conditions in China

Yunlong Guo [a], Shilei Wang [b,*], Guoqing Jing [c], Fei Yang [b], Guixian Liu [b,*], Weile Qiang [b], Yan Wang [b]

[a] Faculty of Civil Engineering and Geosciences, Delft University of Technology, Delft 2628CN, Netherlands
[b] Infrastructure Inspection Research Institute, China Academy of Railway Sciences Co., Ltd., Beijing 100081, China
[c] School of Civil Engineering, Beijing Jiaotong University, Beijing 100044, China

ARTICLE INFO

ABSTRACT

Ballast layer condition should be more regularly and accurately inspected to ensure safe train operation; however, traditional inspection methods cannot sufficiently fulfil this task. This paper presents a method of ground penetrating radar (GPR) application to reflect ballast layer fouling levels under diverse field conditions (annual gross passing load, cleaning and renewal year, fouling composition and transportation type). The results show that the GPR-based inspection method can assess the ballast layer fouling level with a 1–7% difference from the traditional sieving results. Fouling composition (especially metal materials) has a great effect on the GPR signals, thus affecting the inspection accuracy of ballast layer fouling level. Developing diverse GPR-based fouling indicators (by distinguishing different GPR signal features) can improve the GPR inspection applicability to the diverse field conditions.

1. Introduction

Ballast layer is a crucial ballasted track component. Compared with the other components, it occupies the largest volume [1–3]. It has three main important functions: ensuring track stability [4], providing even support to the sleeper and providing drainage for the track. Another function of ballast layer is dissipating the train cyclic loading by the frictions between ballast particles [5,6], through which the train loading is reduced to an acceptable level and then uniformly transmitted to the subgrade [7–9]. The ballast layer is most responsible for track geometry adjustment [10], because other track components (e.g., rail pad) can only correct limited track irregularities [11].

The deformation and deterioration of ballast layer contribute most to the track irregularities [12,13]. Because the ballast layer consists of aggregates with large inhomogeneity, for which uneven deformation frequently occurs [14,15]. On one hand, the uneven deformation of the ballast layer in the vertical direction causes hanging sleepers [16], where the sleeper bottom has no contact with the ballast bed [17]. Hanging sleepers cause rapid damage to all track components, reducing their service lives [18]. More importantly, hanging sleepers affect operation comfort and safety. On the other hand, the uneven deformation in the lateral direction leads to track instability [19,20], because the lateral resistance from the track to the train is almost entirely provided

by the ballast layer [21].

Deterioration of ballast layer leads to track stiffness increment because fouling (normally as small particles) jams the voids in the ballast layer [22]. The jammed ballast layer becomes harder, which means it is losing the elasticity [23]. More importantly, the jammed ballast layer cannot provide sufficient drainage [24]. Rain water can be stored at the ballast-subgrade interface, easily causing ballast pockets [25]. When a train runs on the track with ballast pockets, the water is drawn upward together with the fouling materials (soil, coal, etc.) [26]. This phenomenon is termed as mud pumping [27]. The mud pumping problem has not been properly solved [28]. The ballast layer with mud pumping has already been in an unacceptable condition, and cannot provide desirable performance [5]. Because mud pumping causes that the ballast-ballast contacts are lubricated, and then almost 40% of the shear strength of ballast assemblies can be lost [29]. This leads to very poor operation comfort, and even safety issues [26].

Ballast layer fouling and the corresponding mud pumping are common worldwide track defects [30,31]. To solve this problem, many countries have implemented diverse maintenance regulations for ballast layer [32,33]. For example, in [34,35]ballast layer cleaning and renewal have been used to maintain the ballast layer function by sieving fines out and replacing old ballast particle with new ballast. However, the detailed maintenance schedule/plan/regulation for performing cleaning

---

and renewal actions are not very accurate or precise, which mostly are dependent upon the annual gross passing load (AGPL) and the occurrence of mud pumping (as determined by observation) of ballasted tracks.

In addition, refined strategies are in need of dealing with railway lines under diverse conditions. Several factors can significantly influence fouling generation in ballast layer, such as ballast material, transportation type, maintenance history and environment [36]. The environment means the regions where the tracks are built, such as soft subgrade regions, cold regions, wind-blown sand regions and earthquake regions [37].

To improve ballast layer maintenance, ground penetrating radar (GPR) has been applied to assess the ballast layer fouling level in the last 20 years [6,38–40]. Many studies have been performed on the GPR application methods for ballast layer inspection, including studying the proper radar signal frequency [41–45], processing the radar signal [46–51] and developing accurate indicators to reflect the ballast layer fouling level [35,41,42,52–54]. Limited studies have been performed on the field ballast layer, based on which the fouling levels of field ballast layer were correlated with GPR indicators [55,56]. Very limited studies have attempted to compare these indicators and find the most sensitive indicator to precisely reflect ballast layer fouling level [47]. Few studies have been performed on applying GPR to inspect multiple railway lines, considering diverse railway line conditions [39]. Very few studies were found on analysing the fouling composition in the field ballast layer, studying its influence on the GPR inspection results [42].

Towards these research gaps, this study is performed on multiple field railway lines under diverse conditions, such as diverse AGPLs and transportation types (passenger or freight line). Field ballast layer fouling analysis is performed to calculate the sieving-based fouling index (mass percentage of aggregates passing through certain sieve size [57]), which is compared with the GPR-based fouling index. The influence of fouling composition (especially the metal materials) on GPR inspection quality is focused. Most importantly, the field inspections using GPR have been performed in several regions in China (including soft subgrade region, cold region, mountainous region and earthquake region), which can serve as examples for other countries with ballasted tracks in regions under similar field conditions.

2. Methodology

The methodology includes four parts. The methodology structure is given as follows.

1. GPR equipment and basic principle.
   a. GPR equipment is introduced.
   b. Basic principle of GPR inspection is introduced.
2. Ballast layer fouling indicators based on GPR signals.
   a. Two railway lines used for obtaining GPR signals are introduced.
   b. Five indicators that are used to reflect the ballast layer fouling level are introduced.
   c. Processing the GPR signal (to obtain indicators) is introduced.
   d. Indicator correlation with the fouling index (sieving) is explained to create the GPR-based fouling index.
3. Inspected railway lines. GPR inspection was performed on diverse railway lines, and their field conditions are introduced.
4. Ballast layer sieving-based fouling index results. The fouling index (based on sieving results) is explained.

Note that in this paper, there are two methods to calculate the fouling index. One calculates the index from the sieving results of fouled ballast particles (explained in Section 2.4). The other calculates the index according to the ballast fouling indicators (explained in Section 2.2.4).

2.1. GPR equipment and basic principle

2.1.1. GPR equipment
The GPR equipment was the product from the Geophysical Survey Systems, Inc. (GSSI) in USA. The GPR equipment includes two parts, three antennas (two 2 GHz air-coupled and one 400 MHz ground-coupled antenna) and a data collection unit. For each time of inspection, only one antenna was used to receive the GPR signal. In this paper, the GSSI 2 GHz air-coupled antenna was used as shown in Fig. 1.

The GPR equipment was fixed on a trolley at a height of 400 mm or 190 mm above the ballast layer surface. 400 mm was selected according to the references [58,59]. 400 mm is the most commonly used height. The lowest height for installing the GPR equipment on the inspection train is 190 mm, because the GPR system would be mounted in the future to achieve multiple types of simultaneous track inspections, such as track geometry, rail corrugation and ballast fouling level.

The antennas were placed upon the positions of ballast layer close to the rail (inspected area, Fig. 1) to collect GPR signal. Two reasons were considered for the antenna position: (1) the ballast particles below the rail generate the most fouling after long-term service, and (2) the GPR signals are affected substantially on the condition that antennas are mounted upon the rail. The speed of pushing the trolley is controlled approximately at 3 km/h. The GPR equipment setup is shown in Fig. 1.

To determine the time window, in the first inspection, the data collection unit was set to collect data every 25 ns, as shown in Fig. 2. From the figure, after analysing the GPR signal it can be found that 15 ns is enough to cover the thickness of ballast layer, therefore, for the rest inspections 15 ns was used to obtain more detailed ballast layer information.

2.1.2. Basic principle
Large received GPR signal differences were found between the clean ballast layer and the GPR signal of the fouled ballast layer. The feature diversity of GPR signals can be used to reflect whether the ballast layer is fouled. Furthermore, different ballast layer fouling degrees can be distinguished by featuring the GPR signals, which can be used to indicate the ballast layer fouling level, as explained in the following paragraphs and Section 2.2.

Fig. 2 shows one case of the GPR signal differences between clean ballast layer and fouled ballast layer. The two clean and fouled ballast layers belong to one same railway line but at different segments. The clean ballast layer was cleaned and renewed in 2018, and the fouled ballast layer was cleaned and renewed in 2010.

Fig. 2a shows that the GPR signal of the fouled ballast layer is very different from that of the clean ballast layer. The GPR signal of the fouled ballast layer shows higher amplitudes (see 10–15 ns), and the number of axis crossings (y = 0) is much greater than that of the clean ballast layer.

Fig. 2b shows the power spectrum of the two GPR signals after fast Fourier transform (FFT). The conversion for the time-domain GPR signal into a frequency domain signal through the FFT was introduced in [44]. From Fig. 2b, it can be seen that the power spectrum of the clean ballast layer becomes relatively very small after 2000 MHz. For the fouled ballast layer, the power spectrum still fluctuates after 2000 MHz. In addition, at almost all frequencies, the amplitudes of fouled ballast layer are higher than those of the clean ballast layer.

2.2. GPR-based fouling indicator

In this section, firstly two railway lines that were used to obtain GPR signals are introduced. Afterwards, the calculation means of five indicators are introduced. Then, the validation and sensitive analysis of the indicators were performed. Finally, the method of correlating the indicators with GPR-based fouling index is introduced.

Fig. 1. GPR equipment on ballasted track using 2 GHz antennas.
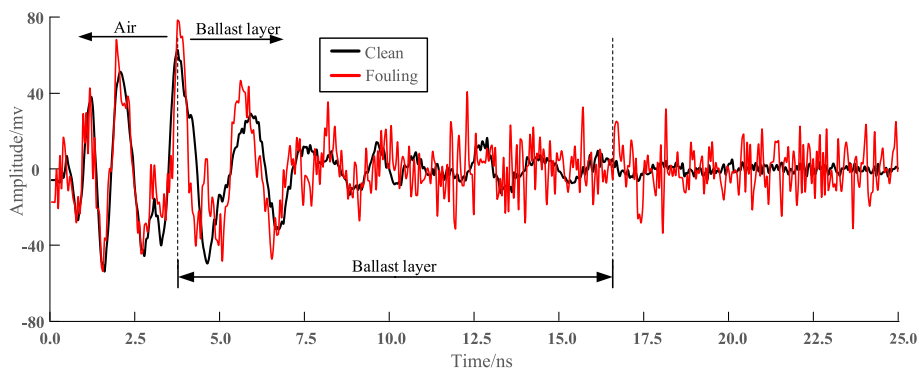
(a) GPR signal (time-domain) of clean and fouled ballast layers
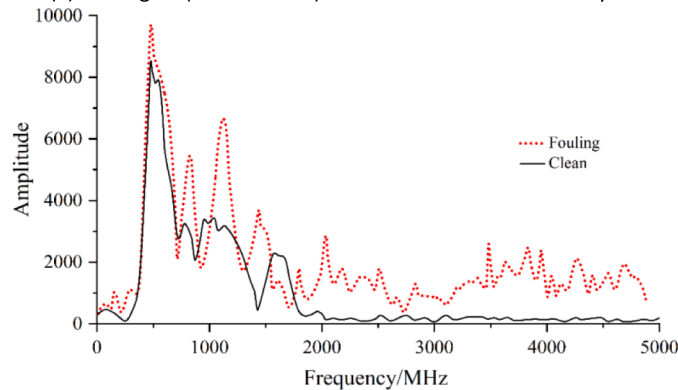
(b) GPR signal spectrum (frequency-domain) of clean and fouled ballast layers

Fig. 2. GPR time-domain signal and frequency-domain signal for clean and fouled ballast layers.

2.2.1. Two railway lines for obtaining GPR signals

Two typical sections were selected from following two railway lines (Lines #5 and #6 in Table 1) to obtain GPR signals and calculate fouling indicators.

- A section in Line #5 was selected because Line #5 is a very busy route in China. There is a clear boundary between two segments (one clean and one fouled) in the section. The clean ballast layer was cleaned and renewed in 2018, while the fouled ballast layer was cleaned and renewed in 2010.
- A section in Line #6 was selected because this section has three kinds of sub-structures supporting the ballasted track, i.e., subgrade,

bridge and tunnel. Figures and further explanations about the two sections are given as follows.

A section of Line #5. The section length is 2100 m. The sleepers are concrete type II mono-block sleepers with spacing at 60 cm. The AGPL is 83 Mt. The GPR inspection was carried out at the beginning of September 2020 (no rainfall in the week prior to the inspection). The ballast shoulder in the fouled segment was found to be heavily fouled. Black fines (coal) were observed when the surface ballast was removed. Vegetation was growing in some locations. The details are shown in Fig. 3.

A section of Line #6. This section is 3 km long with 2 tunnels, as shown in Fig. 4. The tunnel lengths are 1266 m and 137 m, respectively.

Table 1
Inspected railway lines and line conditions.

Line name	Length (km)	Test data	AGPL (Mt)	Year of last cleaning and renewal	Line explanations
#1	3.6	2021/5/24	26	2009	This line is a passenger and freight mixed line, which is a normal railway line used as a reference.
#2	9.0	2021/6/7	–	2013	This line is a new railway line for field tests with almost no traffic, which is used as the reference of clean ballast layer.
#3	9.8	2021/8/27	450	2020	This railway line is served only for coal transportation.
#4	13.0	2021/10/20	17	–	This line is only for passengers. The inspected sections in this line have no special structures. There are no substantial differences along these inspected sections. This railway line is used to compare the GPR results in a line with the same conditions for each section.
	13.0	2021/10/21	17	–	
	3.0	2021/10/22	17	–	
	3.0	2021/10/22	17	–	
#5	2.1	2020/09/03	83	2018	This line is a very busy route in China. Using GPR inspection results from this line, the indicator sensitivity (Section 3.1) can be more easily analysed.
	0.4	2020/09/04	83	2010	
#6	3.0	2020/09/15	37	2019	This line is a first-class general speed railway with subgrade, tunnel and bridge tracks. Using GPR data from this line, the indicator sensitivity (Section 3.1) was analysed for different track structures. The ballast layer in the tunnel section was cleaned in 2019, and the normal section and bridge section have never been cleaned in the most recent 15 years.

Fig. 3. Ballast layer condition of one section in Line #5.

In this section, there are two simple-supported pre-stressed concrete T-beam bridges with lengths at 100 m and 175 m, respectively. The type II mono-block sleeper is used in the subgrade segment, while the tracks in the tunnel and on the bridge segments apply the type III mono-block sleepers. The sleeper spacing is 60 cm. The AGPL of this section is 37 Mt, which is mainly for coal transportation.

The ballast layer in the tunnel segment was cleaned in 2019, and the subgrade and bridge segments have never been cleaned in the past 15 years. The segments without cleaning were experiencing mud-pumping at the crib and shoulder of the ballast layer. The GPR inspection was carried out at the end of September 2020, with no rainfall in the week prior to the inspection.

2.2.2. GPR-based fouling indicator introduction

The obtained time-domain GPR signals and the accordingly converted frequency-domain signals were used to develop five ballast fouling indicators. The GPR indicators are obtained by extracting GPR signal features.

As shown in Fig. 5, the five GPR indicators are calculated by the following features: feature area (SfRa; FFT), scan area (StAb), axis crossings (CrossNum), inflection points (InflecNum) and feature area (after Hilbert transform, HhtAb).

- Spectrum domain integral area (SfRa) is obtained by integrating the spectrum of signal after Fourier transform along the frequency, which is the shadow envelope as shown in Fig. 5 (a).
- The scanning area (StAb) is the scanning area obtained by integrating the absolute value of the time domain signal along the time axis inside the ballast layer, which is the shadow envelope as shown in Fig. 5 (b).
- CrossNum is the number of spectrum line crossing the axis in time domain, which are marked with circles in as shown Fig. 5 (b).
- The inflection points (InflecNum) refers to the number of time-domain signal intersections between increasing and decreasing trend in the ballast layer, which are marked as crossings as shown in in Fig. 5 (b).
- The Hilbert transform is the amplitude envelope area obtained by integrating the time-domain signal inside the ballast layer along the time axis, which is the shadow envelope as shown in Fig. 5 (c). More details about the Hilbert transform can be found in [18].

2.2.3. Indicator validation

The calculation methods of these GPR indicators (detail signal-processing and data-processing means) can be found in [60]. The GPR indicators are validated by checking the indicator values of ballast layers with different fouling levels. Comparison results of the five GPR indicators are shown in Fig. 6. From the figure, it can be seen that the values of the five GPR indicators for the fouled ballast layer are higher than those for the clean ballast layer. This means that the five GPR indicators can reflect the ballast layer fouling level.

In addition, the inflection points (InflecNum) have very similar trend as the axis crossings (CrossNum), thus, their sensitivities are almost the same. Thus, four of the five GPR indicators were analysed on their sensitivities of reflecting the ballast layer fouling level (Section 3.1). The four GPR indicators are SfRa, StAb, CrossNum and HhtAb.

2.2.4. Correlating GPR indicator with sieving-based fouling index

The fouling level of each railway line section was evaluated by using the average, highest and lowest values of the GPR indicators. An example is given in Equation (1). The three types of sub-indicators are calculated with the GPR indicator *StA* (j) In the equations, $j = 1, 2, 3 \ldots n$; n is the total amount of GPR data for the inspected railway line section.

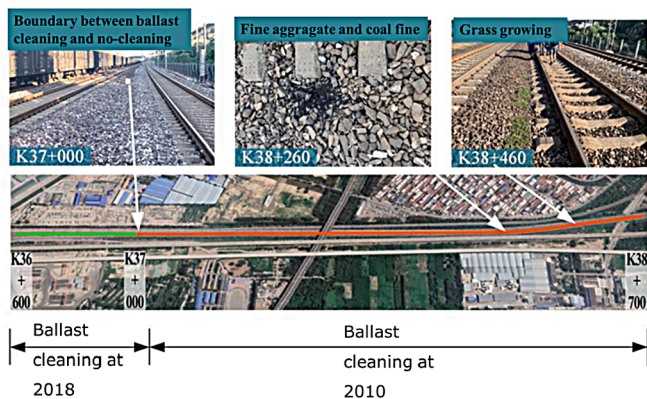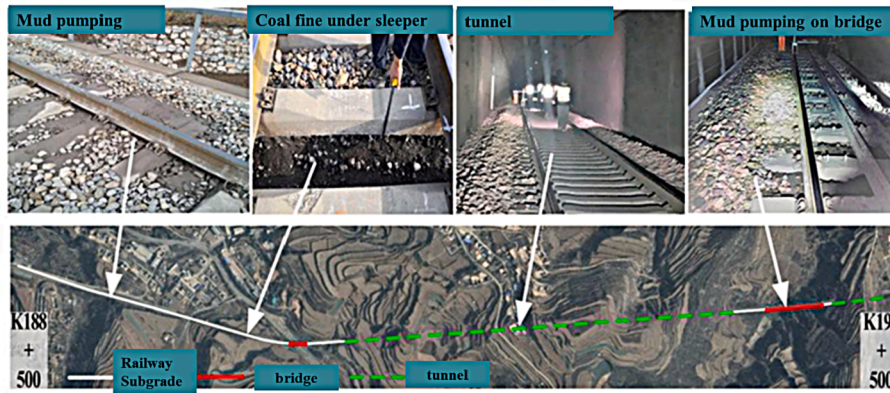$$StAb(average) = \frac{\sum_{j=1}^{n} StAb(j)}{n} \tag{1}$$

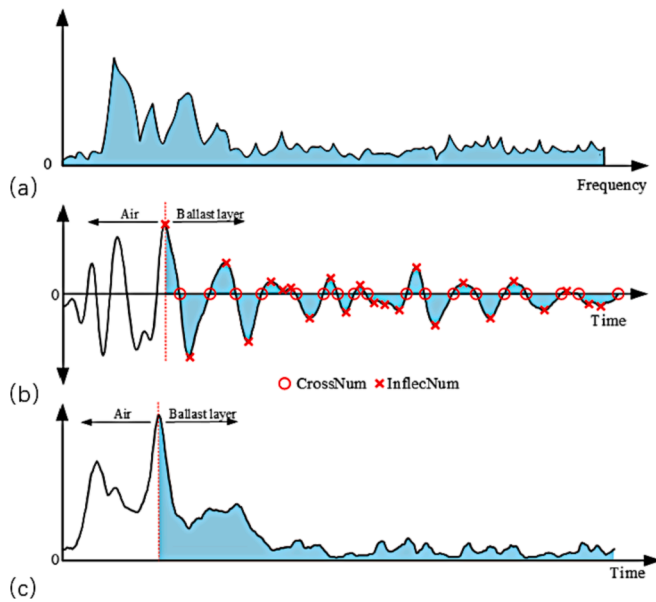**Fig. 4.** Ballast layer conditions of one section in Line #6.

Fig. 5. Indicators produced by processing GPR signal features.

$$StAb(max) = max(StAb(j))$$

$$StAb(min) = min(StAb(j))$$

Eq. (2) presents the correlation between the StAb and the sieving-based fouling index results, explained in Section 2.4. FI_{5mm} and FI_{16mm} are the mass percentages of aggregates passing sieving sizes of 5 mm and 16 mm, respectively. More details about the equations (correlating the indicator with the fouling index based on sieving) can be found in [60].

$$StAb = 3.1 \times 10^5 \times FI_{5mm} - 2.9 \times 10^5 \tag{2}$$

$$StAb = 2.2 \times 10^5 \times FI_{16mm} + 2.0 \times 10^6$$

Using Eq. (1) and Eq. (2), two equations were developed that applied the StAb to calculate the GPR-based fouling index (GFI), as shown in Eq. (3). In the equation, GFI_{5mm} is the estimated mass percentage of aggregates that passes the 5 mm sieve using the StAb; GFI_{16mm} is the estimated mass percentage of aggregates that passes the 5 mm sieve using the StAb.

$$GFI_{5mm}(x) = 2.43 \times StAb(x) \times 10^{-6} + 1.64 \tag{3}$$

$$GFI_{16mm}(x) = 2.61 \times StAb(x) \times 10^{-6} + 13.08$$

To estimate the accuracy of the two GPR-based fouling indices, the sieving-based fouling index is compared with the two indices. The

results are shown in Section 3.2.

2.3. Inspected railway lines

Railway lines under diverse field conditions were inspected, as shown in Fig. 7. Several factors were considered to choose these railway lines, including transportation types, regions, maintenance histories and current ballast layer conditions by observing. The transportation types are the passenger and freight mixed line, new line for field tests and heavy-haul line (used only for coal transportation).

The selected railway lines (Table 1) were cleaned and renewed in different years, and the selected railway line types are different. Details are explained in Table 1.

2.4. Sieving-based fouling index results

In this section, firstly several methods to quantify ballast layer fouling level in the literature are introduced. Afterwards, the reason of choosing the applied fouling index is given. Finally, the procedure of sieving fouled ballast particles (from the field) was explained.

There are several fouling indices to quantify the ballast layer fouling level, such as the percentage of fouling [25,61], percentage void contamination [62] and relative ballast fouling ratio [57,63].

- Percentage of fouling. For example, the Ionescu method to calculate the fouling index is $FI = P_{0.075} + P_{14}$; $P_{0.075}$ represents the cumulative mass passing through a 0.075 mm sieve, while P_{14} denotes the mass of aggregates passing through a 14 mm sieve.
- Percentage void contamination (PVC). The PVC is calculated by $PVC = V_2/V_1$; V_2 indicates voids in ballast, while V_1 is the fouling volume.
- Relative ballast fouling ratio. The relative ballast fouling ratio is calculated by Equation (4). M_f and M_b are the masses of fouling and ballast, respectively, while G_{s-b} and G_{s-f} are the densities of fouling and ballast, respectively.

$$R_{b-f} = \frac{M_f \times (G_{s-b}/G_{s-f})}{M_b} \tag{4}$$

Finally, the relative ballast fouling ratio was chosen for quantifying the ballast layer fouling level because of the following four reasons.

- The percentage of fouling was the most commonly-used fouling index in GPR-related studies.
- In most cases, fouling aggregates below 5 mm are most easily accumulated at the ballast-subgrade interface. Larger particles are not easily shake down.
- Most importantly, sieving the fouled ballast is the fastest way to obtain the fouling level.
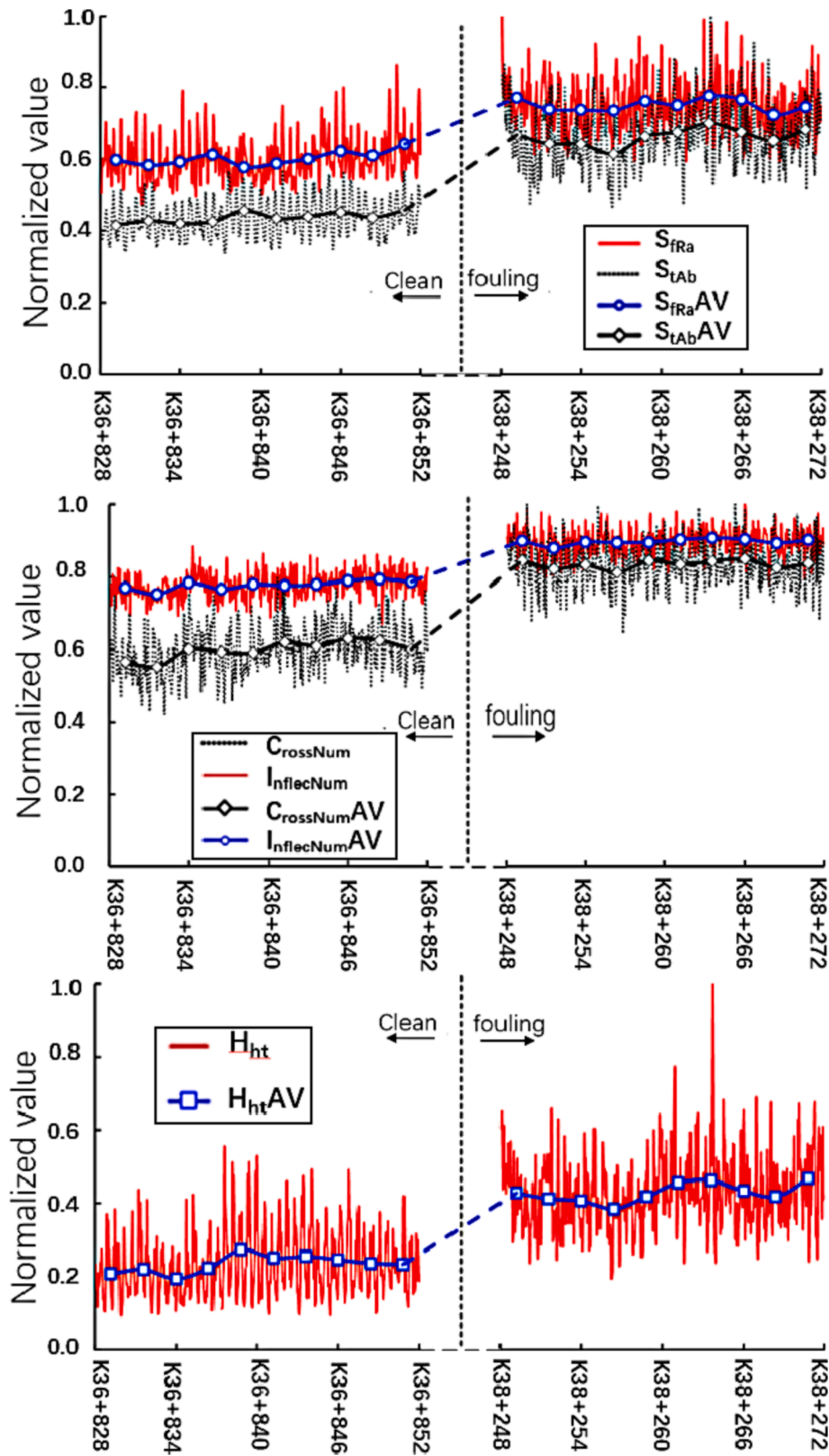
Fig. 6. Ballast layer fouling level presented by five indicators.

- Our method can be considered a simplified relative ballast fouling ratio. According to Eq. (4), when ballast density and fouling density are the same values, the G_{s-b}/G_{s-f} is a constant. In this way, Eq. (4) is the same as Eq. (5).

The fouling index based on sieving (5 mm) used to reflect the fouling level is shown in Eq. (5). It is calculated using the mass percentage of aggregates that are smaller than 5 mm. The calculation methods are the same for the fouling indices using 10 mm and 16 mm sieves. In the equation, m_{5mm} is the weight of particles below 5 mm, and m_{all} is the

Fig. 7. Three examples of railway lines inspected by GPR.

total weight of ballast sample.

$$FI_{5mm} = \frac{m_{5mm}}{m_{all}} \qquad (5)$$

The sieving method for fouled ballast includes four steps: weighing of samples, soaking samples, sieving samples and measuring ballast density. More details of the sieving procedure can be found in [60].

3. Results and discussions

3.1. Indicator application and sensitivity analysis

3.1.1. Indicator application

The Line #4 ballast layer fouling analysis is used for demonstrating the necessity and feasibility of GPR application to ballast layer inspection. Because the ballast layer fouling levels of different segments in one railway line can be very different, even though all the field conditions are almost the same.

The field condition of Line #4 was described in Table 1, some key conditions are summarised as follows.

- Line #4 is a general passenger line in China railways.
- There are no structural differences along these inspected segments in Line #4 (no special structures, no curves, etc.).
- The AGPL and the maintenance histories are almost the same.

However, large differences of ballast layer fouling levels at some locations were found, as shown in Fig. 8. In Fig. 8a, the red and black colours means high fouling levels. At some locations, the ballast layer fouling level is very high. This means that it is unreliable to determine the ballast layer maintenance schedule only by the AGPL.

3.1.2. Indicator sensitivity

The indicator sensitivity analysis is to examine the ability of GPR indicators on reflecting the ballast layer fouling level. A high sensitive GPR indicator changes significantly with a small change of ballast layer fouling level. This is crucial for GPR indicators, especially when using the GPR-based fouling index (calculated by GPR indicator) to reflect ballast layer fouling level in the field. By using the sensitive indicator, the ballast layer fouling level can be evaluated more accurately, according to which precise maintenance schedules can be made.

Fig. 9 shows the results of the four GPR indicators (Line #5). Fig. 9a shows the GPR signal using traditional signal processing method, which is difficult to visually identify the ballast layer fouling level. This is greatly improved after performing the Hilbert transform (explained in Section 2.2.2), as shown in Fig. 9b. The green colour has the lowest amplitude (low fouling level), and the black colour has the highest amplitude (high fouling level). It can be observed that more black colour is in the sections K38 + 100 − K38 + 500, which is consistent with the sieving results of the dug ballast samples from the field.

Because this railway line section has same AGPL and year of cleaning and renewal, finding out the reason of high ballast layer fouling level
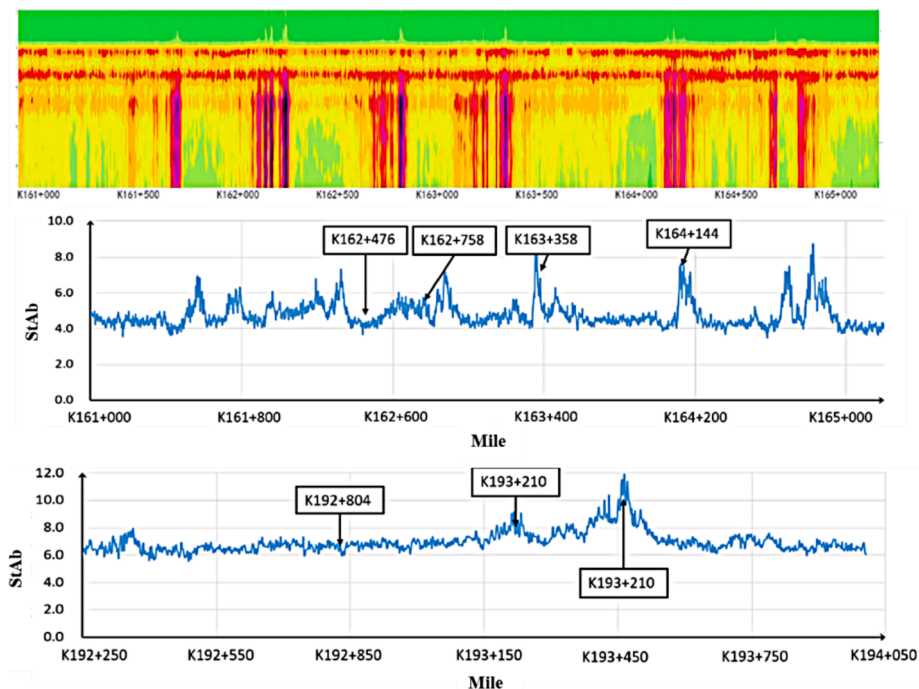

Fig. 8. GPR results of Line #4.

a. GPR signal with traditional signal processing method

b. GPR signal processed by Hilbert transform

c. Four GPR indicators to present ballast layer fouling level
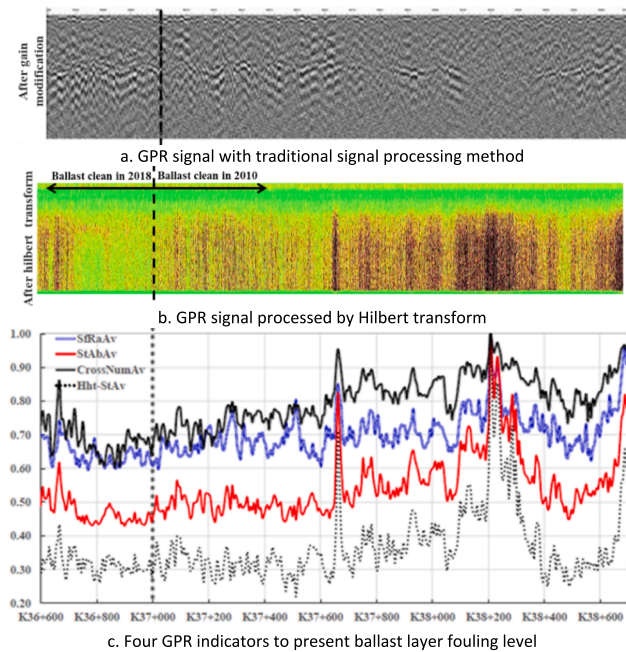
Fig. 9. Indicators from the GPR signal for Line #5.

was performed. It was found that this section is located within the radius of a 2500 m curve. The rapid ballast layer fouling results from the centrifugal force on ballast particles (induced by the train passing the curve) and the freight dropping into the ballast layer. This means that the track structures under abnormal loading (e.g., curve, transition zone and turnout) have great influence on ballast layer fouling generation. Specifically, the curve, transition zone and turnout are special structures where impact loading usually occurs. The impact loading leads to differential settlements of ballast layer, which causes higher sleeper stress to the ballast layer, accelerating ballast degradation.

As shown in Fig. 9c, the four GPR indicators are compared. It can be seen that the four GPR indicators have the same trend. In particular, SfRa and CrossNum present almost the same values, for which in the following analysis the three GPR indicators (StAb, CrossNum and HhtAb) are used.

The GPR indicator sensitivity is analysed by comparing the maximum indicator value, minimum indicator value and the ratio of the maximum to the minimum values, as shown in Table 2. The ratio of HhtAb is 4.6, which is the most sensitive GPR indicator. The second sensitive GPR indicator is the StAb.

From the table, it can also be observed that the sensitivity of these GPR indicators is effected by the minimum indicator value. This is also helpful for the future field ballast layer inspection. Because high ballast layer fouling level can even be observed by eye. However, the fouling normally accumulates at the ballast-subgrade interface, which is hard to be observed. Using this sensitive indicator, small fouling level at the initial stage can be detected.

The GPR indicator results of the 3 km section in Line #6 are shown in Fig. 10. The sensitivities of the three GPR indicators (StAb, CrossNum and HhTAb) are consistent with the analysis of Line #5. HhtAb is the most sensitive indicator, followed by the StAb.

Table 2
Sensitivity of different GPR signal indicators.

Name	SfRa	StAb	CrossNum	HhtAb
Maximum value	1.00	1.00	1.00	1.00
Minimum value	0.60	0.43	0.60	0.22
Ratio of maximum value to minimum values	1.7	2.3	1.7	4.6

Regarding the influence of different sub-structures on ballast layer fouling level, results show that ballast cleaning and renewal play more decisive role than the sub-structure differences.

- The three GPR indicators (StAb, CrossNum and HhTAb) all show high values for the segment of K188 + 500 − K188 + 750. The reason can be that this segment has not been cleaned or renewed for the last 15 years. This means that ballast cleaning and renewal primarily effect the ballast layer fouling level.
- In the tunnel segment, the values of the three GPR indicators are relatively low. The reason can be that the tunnel segment was cleaned and renewed 2 years ago.
- In the bridge segment, the values of StAb and CrossNum are high due to the long absence of ballast cleaning and renewal.

In summary, by comparing these GPR indicators, the StAb can be suitable for ballast layers on the subgrade, bridge and tunnel. Because StAb has the acceptable sensitivity for ballast layer fouling inspection on these sub-structures. In addition, the StAb saves computational costs and can rapidly reflect ballast layer conditions. Specifically, the calculation of HhtAb involves empirical modal decomposition, the calculation requires a longer time than the others. Specifically, the calculation time costs 140 s for 1 km with the HhtAb, while only 5 s are required for the other three indicators. Therefore, the StAb is used in the following analysis, which compares the GPR-based fouling index (calculated by StAb) with the fouling index (based on sieving results).

3.2. GPR-based fouling index validation and application

The GPR-based fouling index is validated by comparing the index values with the sieving-based fouling index values. Specifically, using the sieving method described in Section 2.4, sieving-based fouling index results of 5 mm and 16 mm (Line #3 and Line #4) are obtained. The GPR-based fouling index values of Line #3 and Line #4 are calculated using Equations 1–3 and the StAb values.

After the GPR-based fouling index is validated, some abnormal GPR-based fouling index values from Line #3 are analysed due to its unusual fouling composition. The fouling composition of Line #1 and Line #2 was used as references.

3.2.1. Index validation

In Table 3 and Table 4, the GPR-based fouling index values are all greater than the fouling index (sieving), with value difference ranging from −1% to 2% for the 5 mm sieving size and −1% to 7% for the 16 mm sieving size. The value difference is calculated by the GPR-based fouling index minus the sieving-based fouling index. The value difference is small, which means that GPR can accurately reflect the ballast layer fouling level. In addition, the applied indicator (StAb) and the signal processing methods are validated.

3.2.2. Fouling composition analysis

Table 5 and Table 6 show that the GPR-based fouling index values are all greater than the fouling index (sieving), with value differences from 1% to 10% for the 5 mm sieving size, while the value differences for 16 mm are from 7% to 18%.

There are some abnormal GPR-based fouling index values, which means that the value differences of Line #3 are larger than those of Line #4. The following factors are analysed.

- GPR equipment. In practice, during GPR testing on these railway lines (Section 2.1), no changes were made to the GPR system consisting of the antennas, mainframe, etc., so the large value difference is not caused by GPR equipment.
- Sieving results. The sieving process was rigorously kept the same, so the difference is not caused by the sieving error.
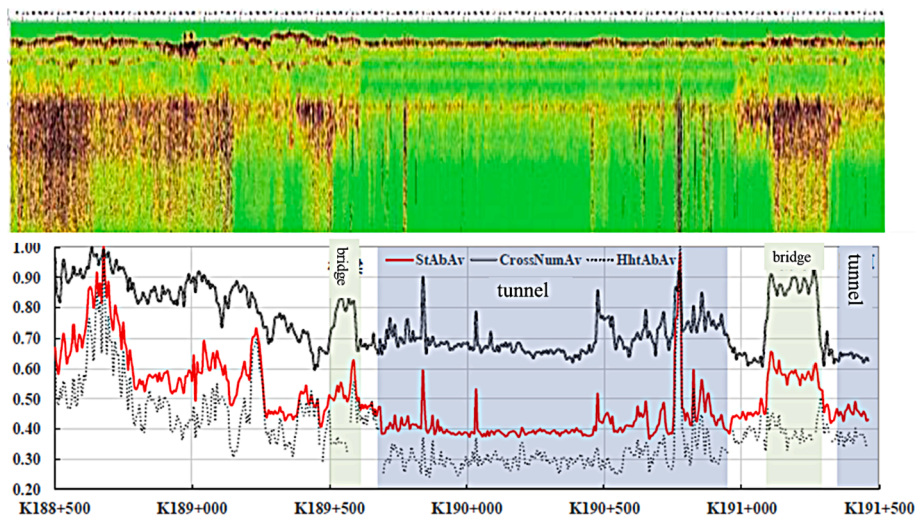
Fig. 10. Line #6 GPR inspection results.

Table 3
Fouling indices for Line #4 (5 mm sieve size passing rate and GPR).

Location (section mark)	Fouling index (sieving)	Fouling index (GPR)	Difference value
K162 + 470	4.16	4.57	0.41
K162 + 476	3.75	4.71	0.96
K162 + 482	3.62	4.55	0.94
K162 + 752	2.89	4.80	1.91
K162 + 758	3.47	5.39	1.92
K162 + 764	4.15	5.48	1.33
K163 + 352	7.09	5.63	−1.46
K163 + 358	4.84	7.04	2.20
K163 + 364	5.22	6.67	1.45
K164 + 138	7.12	6.17	−0.96
K164 + 144	4.04	6.46	2.42
K164 + 150	8.02	6.37	−1.65
K192 + 860	8.45	6.28	−2.17
K192 + 866	6.02	6.40	0.37
K193 + 210	7.01	7.06	0.05
K193 + 450	6.51	8.53	2.02
K193 + 456	8.23	8.11	−0.12

Table 4
Fouling indices for Line #4 (16 mm sieve size passing rate and GPR).

Location (section mark)	Fouling index (sieving)	Fouling index (GPR)	Difference value
K162 + 470	13.28	16.22	2.94
K162 + 476	13.28	16.38	3.10
K162 + 482	11.07	16.21	5.14
K162 + 752	8.97	16.47	7.50
K162 + 758	10.24	17.10	6.87
K162 + 764	11.56	17.20	5.64
K163 + 352	16.85	17.36	0.51
K163 + 358	13.55	18.87	5.32
K163 + 364	14.21	18.48	4.27
K164 + 138	16.55	17.94	1.38
K164 + 144	9.13	18.25	9.12
K164 + 150	17.42	18.15	0.73
K192 + 860	19.34	18.06	−1.28
K192 + 866	15.26	18.19	2.92
K193 + 210	18.09	18.89	0.81
K193 + 450	15.22	20.47	5.25
K193 + 456	19.09	20.03	0.94

- Fouling composition. The fouling material composition analysis was performed with Line #1 (reference), Line #2 (reference) and Line #3.

Table 5
Fouling indices for Line #3 (5 mm sieve size passing rate and GPR).

Location (section mark)	Fouling index (sieving)	Fouling index (GPR)	Difference value
K270 + 867	3.84	14.06	10.22
K270 + 887	6.75	13.75	7.00
K271 + 113	5.99	9.56	3.57
K271 + 118	7.97	9.44	1.47
K271 + 200	13.91	15.19	1.28
K271 + 218	6.72	13.41	6.69
K271 + 226	7.88	13.97	6.09
K271 + 304	5.03	15.55	10.52
K271 + 314	6.24	16.34	10.10
K271 + 324	6.25	16.53	10.28

Table 6
Fouling indices for Line #3 (16 mm sieve size passing rate and GPR).

Location (section mark)	Fouling index (sieving)	Fouling index (GPR)	Difference value
K270 + 867	8.00	26.41	18.41
K270 + 887	13.91	26.08	12.17
K271 + 113	10.92	21.58	10.65
K271 + 118	14.43	21.45	7.02
K271 + 200	19.62	27.62	8.00
K271 + 218	12.61	25.72	13.10
K271 + 226	14.71	26.31	11.61
K271 + 304	10.58	28.01	17.43
K271 + 314	13.56	28.85	15.29
K271 + 324	13.38	29.06	15.68

For Line #3, the specific ballast fouling composition analysis method is given as follows. Four fouled ballast layer samples at two different locations (K270 + 867 and K271 + 113) were selected for fouling composition analysis, as shown in Table 7. The two locations were

Table 7
Ballast fouling composition and content for Line #3.

Location	Difference value (16 mm)	Sample number	Weight of ballast with iron ore (kg)	Other composition weight (kg)	Weight percentage of the iron ore
K270 + 867	18.41	1	22.47	6.91	77%
		2	8.93	2.28	80%
K271 + 113	10.65	3	5.39	23.65	19%
		4	5.96	20.87	22%

selected because the value differences (18.41 and 10.65) are very large compared to the others. The results show that the ballast samples of Line #3 have a very high content of iron ore, while the iron ore was not found in the samples of Line #1 or Line #2.

Due to the metallic composition of the iron ore, more energy reflection of radar electromagnetic waves occurred in the ballast layer, which leads to an increase in the GPR signal fluctuations. Then, the GPR-based fouling index becomes higher value, because it is calculated using the GPR indicator, which is obtained by featuring these GPR signal fluctuations.

In summary, the GPR-based indicator can be used for inspecting ballast layer fouling level. In addition, it can be found that the fouling composition has great influence on the GPR-based fouling index (by influencing the GPR signal fluctuations). Therefore, more focuses can be on this GPR application development direction. For example, the research direction can be the use of GPR signals to analyse detailed ballast fouling composition, e.g., water, metal, etc.

3.3. Ballast layer field condition analysis

The railway lines are inspected using GPR and the GPR-based fouling index are calculated using Eqs. (1)–(3). The GPR-based fouling index, sieving-based fouling index and their filed conditions are compared. The field conditions include AGPL, cleaning and renewal year for each railway line, as shown in Table 8.

The table shows that the ballast layer fouling level mostly depends on the cleaning and renewal year and the AGPL, nevertheless, the railway line type also has great effects on the ballast layer fouling level.

For example, in the railway lines for freight transportation, higher fouling level is observed. For example, Line #3 is a special line for coal transportation in China. The line was cleaned and renewed in October 2020, and GPR inspection was performed after only one year. However, the fouling level is higher than Line #4 (passenger only) and Line #2 (railway line for field tests).

Even though cleaning and renewal year dominate the influence on ballast layer fouling level, the prediction of maintenance schedule is still not easy only using these two conditions. Specifically, Line #4 and Line #2 were cleaned and renewed in the same year, and the volume of traffic on Line #4 was greater than that on Line #2. However, the difference in fouling level (both 5 mm and 16 mm) of Line #4 and Line #2 is not significant. Therefore, for the same railway line, it is regular that the fouling level increases with the increasing of cleaning and renewal year and AGPL, but the fouling level is not directly proportional to the cleaning and renewal year or AGPL. This means that it is not possible to determine the fouling level only by combining cleaning and renewal year and AGPL.

GPR inspection and sieving results for each railway line show that the fouling level in most of the inspected lines is uniform. However, some locations/segments have significantly higher fouling level. The length of these locations/segments ranges from tens of metres to hundreds of metres. Although these railway line sections have not met the threshold of cleaning and renewal (stipulated in standards [34]), their ballast layer fouling level has already been quite high. This demonstrates the importance of applying GPR for future ballast layer inspection. In addition, the necessity of creating standards of GPR application with consideration of diverse railway line conditions is also demonstrated.

4. Conclusions and perspectives

4.1. Conclusions

In this paper, the application of GPR to ballast layer fouling assessment is studied, especially to the ballast layers under diverse field conditions. Different GPR indicators reflecting ballast layer fouling level are analysed on their sensitivities. Afterwards, using one indicator, a GPR-based fouling index is developed. The GPR-based index is validated with the sieving-based fouling index, and then the GPR-based fouling index is used to analyse fouling level of multiple railway lines under diverse field conditions. The factors influencing the GPR fouling index results are analysed, such as the fouling composition. After performing this study, the conclusions are given as follows.

- A good correlation between the GPR-based fouling index and the sieving-based fouling index was found. This means that GPR is very promising for ballast layer fouling inspection.
- The GPR-based fouling index (calculated with the indicator StAb) is the most suitable index for ballast layer fouling evaluation, because the difference between the GPR-based fouling index and the sieving-based fouling index is small.
- Fouling material has a great influence on the GPR-based fouling index, especially in the case of iron ore, because it has big influence on the GPR signal fluctuations.

4.2. Limitations and future perspectives

After performing this study, some limitations were observed in this study, which are given as follows.

From the sensitivity analysis, it can be seen that the applicable GPR indicator can be StAb, but it is not a perfect one. The five GPR indicators used in this study are sensitive to different conditions. For example, in the bridge segment (Fig. 10), the CrossNum and StAb are more sensitive than the HhtAb. HhtAb can better represent ballast layer fouling level by colours; however, it cannot perfectly reflect the ballast layer fouling level on bridges. This indicates that different indicators can have different sensitivities to different sub-structures for tracks. Therefore, it is better to combine these indicators or develop another means of signal processing, by which a new comprehensive GPR indicator can be developed. Because relevant studies using data science are blooming,

Table 8
Annual gross passing load, cleaning and renewal year and fouling level for each railway line.

Line	Cleaning and renewal year	AGPL (Mt/year)	Sieve size (mm)	Fouling index (GPR)			Fouling index (sieving)	
				Max	Min	Av	Max	Min
#1	2008	26	5	20.95	8.49	12.99	18	10
			16	33.81	20.43	25.26	29	21
			25	51.73	38.43	43.23	53	37
#2	2010	Very low	5	18.11	5.14	7.46	9	4
			16	30.76	16.84	19.32	16	7
			25	48.70	34.86	37.33	44	27
#3	2020	450	5	–	–	–	15	4
			16	–	–	–	20	8
			25	–	–	–	31	20
#4	2008	17	5	5.61	3.25	3.83	8	3
			16	17.35	14.80	15.43	19	9
			22.5	35.36	32.83	33.46	32	15

then using the most suitable algorithm to develop the most sensitive indicator is a promising research direction.

Further development of GPR signal analysis to identify fouling composition is necessary. The ballast fouling compositions vary in general. However, only the iron ore was analysed in this study, because it has the largest influence on the GPR-based fouling index. Regarding other fouling materials, such as water, coal and sands, it is a very good research direction to identify them as well. In particular, coal is the main fouling material in coal transportation lines not only in China, but also in other countries (e.g., Australia), while sand is the main contamination in ballast layers in desert areas.

In addition, the ballast layer moisture has great impact on the GPR signals, as the recently released report stated, see [64]. More focuses can be put on this research direction. The moderate-frequency GPR can better identify the moisture in the ballast layer. Therefore, the combination of high-frequency and moderate-frequency GPR can be considered.

A study was performed on correlating the GPR-based fouling index with ballasted track geometry deterioration. The correlation is under investigation according to our current inspection data. More filed inspection data analysis (including rail-related data) has been performed on this, and next publication will be on this topic.

Even though several railway lines were inspected and some GPR inspection results were analysed, the data are still not sufficient for a deeper analysis on the ballast layer deformation. In the next step, GPR inspection will be used for long-term inspection, mainly on ballast-related track settlement. This is very helpful for ballast layer maintenance guidance.

The GPR-based fouling index was only correlated with one kind of sieving-based fouling index. The PVC and relative ballast fouling ratio can reflect the void percentage of the ballast layer, and the working principle of high-frequency GPR is to detect the voids in ballast layer. Therefore, correlating the GPR-based fouling index with all of these kinds of sieving-based fouling indices is an interesting research direction.

CRediT authorship contribution statement

Yunlong Guo: Writing – original draft, Writing – review & editing. **Shilei Wang:** Formal analysis, Investigation, Software, Visualization, Funding acquisition. **Guoqing Jing:** Coordination, Supervision. **Fei Yang:** Data curation. **Guixian Liu:** Funding acquisition, Resources. **Weile Qiang:** Formal analysis, Validation. **Yan Wang:** Formal analysis, Investigation.

Declaration of Competing Interest

The authors declare that they have no known competing financial interests or personal relationships that could have appeared to influence the work reported in this paper.

Acknowledgements

References

[1] H.M. Jol, Ground penetrating radar theory and applications, elsevier 2008.
[2] W. Zhai, Vehicle–track coupled dynamics theory and applications, Springer Singapore (2020).
[3] B. Indraratna, T. Ngo, Ballast railroad design: smart-uow approach, CRC Press, 2018.
[4] Y. Guo, L.u. Zong, V. Markine, X. Wang, G. Jing, Experimental and numerical study on lateral and longitudinal resistance of ballasted track with nailed sleeper, International Journal of Rail Transportation 10 (1) (2022) 114–132.
[5] B. Indraratna, W. Salim, C. Rujikiatkamjorn, Advanced rail geotechnology: Ballasted track, CRC Press London, 2011.
[6] D. Read, A. Meddah, D. Li, W. Mui, Ground penetrating radar technology evaluation on the High Tonnage Loop: phase 1, 2017.
[7] Y. Guo, V. Markine, J. Song, G. Jing, Ballast degradation: Effect of particle size and shape using Los Angeles Abrasion test and image analysis, Construction and Building Materials 169 (2018) 414–424.
[8] J. Xiao, Y. Wang, D. Zhang, X. Zhang, J. Guo, Testing of Contact Stress at Ballast Bed-Soil Subgrade Interface under Cyclic Loading Using the Thin-Film Pressure Sensor, Journal of Testing and Evaluation 48 (3) (2020) 20190171.
[9] L. Xu, W. Zhai, Train–track coupled dynamics analysis: system spatial variation on geometry, physics and mechanics, Railway Engineering Science (2020) 1–18.
[10] Y. Guo, V. Markine, G. Jing, Review of ballast track tamping: Mechanism, challenges and solutions, Construction and Building Materials 300 (2021).
[11] S. Kaewunruen, A.M. Remennikov, Sensitivity analysis of free vibration characteristics of an in situ railway concrete sleeper to variations of rail pad parameters, Journal of Sound and Vibration 298 (1–2) (2006) 453–461.
[12] A. Danesh, M. Palassi, A.A. Mirghasemi, Evaluating the influence of ballast degradation on its shear behaviour, International Journal of Rail Transportation 6 (3) (2018) 145–162.
[13] E. Tutumluer, Y. Qian, Y.M.A. Hashash, J. Ghaboussi, D.D. Davis, Discrete element modelling of ballasted track deformation behaviour, International Journal of Rail Transportation 1 (1–2) (2013) 57–73.
[14] B. Indraratna, Y. Sun, S. Nimbalkar, Laboratory assessment of the role of particle size distribution on the deformation and degradation of ballast under cyclic loading, Journal of Geotechnical and Geoenvironmental Engineering 142 (7) (2016) 04016016.
[15] B. Indraratna, S. Nimbalkar, C. Rujikiatkamjorn, From theory to practice in track geomechanics – Australian perspective for synthetic inclusions, Transportation Geotechnics 1 (4) (2014) 171–187.
[16] M. Sol-Sanchez, F. Moreno-Navarro, M.C. Rubio-Gamez, The Use of Deconstructed Tires as Elastic Elements in Railway Tracks, Materials (Basel) 7 (8) (2014) 5903–5919.
[17] M. Sysyn, M. Przybylowicz, O. Nabochenko, J. Liu, Mechanism of Sleeper-Ballast Dynamic Impact and Residual Settlements Accumulation in Zones with Unsupported Sleepers, Sustainability 13 (14) (2021) 7740.
[18] R. Roberts, I. Al-Audi, E. Tutumluer, J. Boyle, Subsurface Evaluation of Railway Track Using Ground Penetrating Radar (2008).
[19] J.A. Zakeri, Y. Bahari, K. Yousefian, Experimental investigation into the lateral resistance of Y-shape steel sleepers on ballasted tracks, Proceedings of the Institution of Mechanical Engineers, Part F: Journal of Rail and Rapid Transit 235 (8) (2021) 917–924.
[20] L. Le Pen, A.R. Bhandari, W. Powrie, Sleeper End Resistance of Ballasted Railway Tracks, Journal of Geotechnical and Geoenvironmental Engineering 140 (5) (2014) 04014004.
[21] C. Ngamkhanong, C.M. Wey, S. Kaewunruen, Buckling Analysis of Interspersed Railway Tracks, Applied Sciences 10 (9) (2020) 3091.
[22] M. Esmaeili, J.A. Zakeri, S.A. Mosayebi, Effect of sand-fouled ballast on train-induced vibration, International Journal of Pavement Engineering 15 (7) (2013) 635–644.
[23] M. Esmaeili, P. Aela, A. Hosseini, Experimental assessment of cyclic behavior of sand-fouled ballast mixed with tire derived aggregates, Soil Dynamics and Earthquake Engineering 98 (2017) 1–11.
[24] H. Huang, M. Moaveni, S. Schmidt, E. Tutumluer, J.M. Hart, Evaluation of Railway Ballast Permeability Using Machine Vision-Based Degradation Analysis, Transportation Research Record 2672 (10) (2018) 62–73.
[25] E.T. Selig, J.M. Waters, Track geotechnology and substructure management, Thomas Telford (1994).
[26] C. Kuo, C. Hsu, Y. Chen, C. Wu, H. Wang, D. Chen, Y. Lin, Using Ground-penetrating Radar to Promote the Investigating Efficiency in Mud Pumping Disaster of Railways, Proceedings of Engineering and Technology Innovation 4 (2016) 49.
[27] T.T. Nguyen, B. Indraratna, R. Kelly, N.M. Phan, F. Haryono, Mud pumping under railtracks: mechanisms, assessments and solutions, (2019).
[28] S. Chawla, J.T. Shahu, Reinforcement and mud-pumping benefits of geosynthetics in railway tracks: Numerical analysis, Geotextiles and Geomembranes 44 (3) (2016) 344–357.
[29] B. Indraratna, D. Ionescu, H. Christie, Shear behavior of railway ballast based on large-scale triaxial tests, Journal of geotechnical and geoenvironmental Engineering 124 (5) (1998) 439–449.
[30] M. Koohmishi, M. Palassi, Effect of gradation of aggregate and size of fouling materials on hydraulic conductivity of sand-fouled railway ballast, Construction and Building Materials 167 (2018) 514–523.
[31] R. De Bold, D.P. Connolly, S. Patience, M. Lim, M.C. Forde, Using impulse response testing to examine ballast fouling of a railway trackbed, Construction and Building Materials 274 (2021) 121888.
[32] B.s.p.B.E., British Standards Institution, Aggregates for railway ballast, British Standards Institution London (2013).
[33] R. Nålsund, Railway ballast characteristics, selection criterion and performance, Norwegian University of Science and Technology, Trondheim, Department of Civil and Transport Engineering, 2014.
[34] C.R.I.C. Ltd General railway line maintenance rules 2019 Beijing.

[35] J. Sadeghi, M.E. Motieyan-Najar, J.A. Zakeri, B. Yousefi, M. Mollazadeh, Improvement of railway ballast maintenance approach, incorporating ballast geometry and fouling conditions, Journal of Applied Geophysics 151 (2018) 263–273.

[36] A. Hudson, G. Watson, L. Le Pen, W. Powrie, Remediation of Mud Pumping on a Ballasted Railway Track, Advances in Transportation Geotechnics Iii 143 (2016) 1043–1050.

[37] J.A. Zakeri, M. Esmaeili, M. Fathali, Evaluation of humped slab track performance in desert railways, Proceedings of the Institution of Mechanical Engineers, Part F: Journal of Rail and Rapid Transit 225 (6) (2011) 566–573.

[38] K.M. Scanlan, M.T. Hendry, C.D. Martin, D.R. Schmitt, A Review of Methods for Estimating Ballast Degradation Using Ground-Penetrating Radar, in: T.D. Stark, R. H. Swan, R. Szecsy (Eds.), Railroad Ballast Testing and Properties, ASTM International, 100 Barr Harbor Drive, PO Box C700, West Conshohocken, PA 19428-2959, 2018, pp. 54–76.

[39] C. Basye, S.T. Wilk, Y. Gao, Ground Penetrating Radar (GPR) Technology and Evaluation Implementation, United States. Department of Transportation, Federal Railroad Administration, 2020.

[40] B.E. Barrett, H. Day, J. Gascoyne, A. Eriksen, Understanding the capabilities of GPR for the measurement of ballast fouling conditions, Journal of Applied Geophysics 169 (2019) 183–198.

[41] A. Benedetto, F. Tosti, L. Bianchini Ciampoli, A. Calvi, M.G. Brancadoro, A. M. Alani, Railway ballast condition assessment using ground-penetrating radar – An experimental, numerical simulation and modelling development, Construction and Building Materials 140 (2017) 508–520.

[42] S.S. Artagan, V. Borecky, Advances in the nondestructive condition assessment of railway ballast: A focus on GPR, NDT E Int. 115 (2020) 102290.

[43] M. Clark, R. Gillespie, T. Kemp, D. McCann, M. Forde, Electromagnetic properties of railway ballast, NDT E Int. 34 (5) (2001) 305–311.

[44] F. Tosti, L. Bianchini Ciampoli, A. Calvi, A.M. Alani, A. Benedetto, An investigation into the railway ballast dielectric properties using different GPR antennas and frequency systems, NDT E Int. 93 (2018) 131–140.

[45] F. De Chiara, S. Fontul, E. Fortunato, GPR Laboratory Tests For Railways Materials Dielectric Properties Assessment, Remote Sensing 6 (10) (2014) 9712–9728.

[46] M. Silvast, A. Nurmikolu, B. Wiljanen, M. Levomaki, An Inspection of Railway Ballast Quality Using Ground Penetrating Radar in Finland, Proceedings of the Institution of Mechanical Engineers, Part F: Journal of Rail and Rapid Transit 224 (5) (2010) 345–351.

[47] R. De Bold, G. O'Connor, J.P. Morrissey, M.C. Forde, Benchmarking large scale GPR experiments on railway ballast, Construction and Building Materials 92 (2015) 31–42.

[48] P. Shangguan, I.L. Al-Qadi, Z. Leng, Ground-Penetrating Radar Data to Develop Wavelet Technique for Quantifying Railroad Ballast-Fouling Conditions,

[49] Transportation Research Record: Journal of the Transportation Research Board 2289 (1) (2012) 95–102.

[49] C. Bianchini, Calvi, D'Amico, Railway Ballast Monitoring by Gpr: A Test Site Investigation, Remote Sensing 11 (20) (2019) 2381.

[50] L. Bianchini Ciampoli, F. Tosti, N. Economou, F. Benedetto, Signal Processing of GPR Data for Road Surveys, Geosciences 9 (2) (2019) 96.

[51] P. Anbazhagan, S. Lijun, I. Buddhima, R. Cholachat, Model track studies on fouled ballast using ground penetrating radar and multichannel analysis of surface wave, Journal of Applied Geophysics 74 (4) (2011) 175–184.

[52] I.L. Al-Qadi, W. Xie, R. Roberts, Scattering analysis of ground-penetrating radar data to quantify railroad ballast contamination, NDT E Int. 41 (6) (2008) 441–447.

[53] Q. Zhang, A. Eriksen, J. Gascoyne, Z. Rail, Rail radar-a fast maturing tool for monitoring trackbed, Proceedings of the XIII Internarional Conference on Ground Penetrating Radar, IEEE, 2010, pp. 1-5.

[54] A. Eriksen, J. Gascoyne, R. Fraser, Ground penetrating radar as part of a holistic strategy for inspecting trackbed, Aust. Geomech. Soc 46 (3) (2011) 1–11.

[55] L.B. Ciampoli, A. Calvi, E. Oliva, Test-site operations for the health monitoring of railway ballast using Ground-Penetrating Radar, Transp. Res. Procedia 45 (2020) 763–770.

[56] M. Brough, A. Stirling, G. Ghataora, K. Madelin, Evaluation of railway trackbed and formation: a case study, NDT E Int. 36 (3) (2003) 145–156.

[57] B. Indraratna, L.-J. Su, C. Rujikiatkamjorn, A new parameter for classification and evaluation of railway ballast fouling, Can. Geotech. J. 48 (2) (2011) 322–326.

[58] F. Tosti, A. Benedetto, A. Calvi, L.B. Ciampoli, Laboratory investigations for the electromagnetic characterization of railway ballast through GPR, Ground Penetrating Radar (GPR), in: 2016 16th International Conference on, 2016, pp. 1–6.

[59] I. Al-Qadi, W. Xie, R. Roberts, Optimization of antenna configuration in multiple-frequency ground penetrating radar system for railroad substructure assessment, NDT E Int. 43 (1) (2010) 20–28.

[60] Y. Guo G. Liu G. Jing J. Qu S. Wang W. Qiang Ballast fouling inspection and quantification with ground penetrating radar (GPR) 1 18.

[61] D. Ionescu, Ballast degradation and measurement of ballast fouling, Seventh Railway Engineering Conference, Commonwealth Institute, London, 2004.

[62] F. Feldman, D. Nissen, Alternative testing method for the measurement of ballast fouling: percentage void contamination, CORE 2002, Cost Efficient Railways through Engineering, Conference on Railway Engineering, Wollongong, New South Wales, November 10-13, 2002, 2002.

[63] P. Anbazhagan, T. Bharatha, G. Amarajeevi, Study of ballast fouling in railway track formations, Indian Geotech. J. 42 (2) (2012) 87–99.

[64] S. Kulesza, M.L. Barry, R.R. Sherwood, A. Santos, Unsaturated Characteristics of Fouled Ballast to Support In Situ Identification of Fouling Using Ground Penetrating Radar–Phase I, United States. Department of Transportation. Federal Railroad Administration, 2022.